HHS Public Access

Author manuscript

Mol Pharm. Author manuscript; available in PMC 2023 January 17.

Published in final edited form as:

Mol Pharm. 2020 October 05; 17(10): 3900–3914. doi:10.1021/acs.molpharmaceut.0c00641.

Acute Immune Response of Micro- and Nanosized Erythrocyte-Derived Optical Particles in Healthy Mice

Taylor M. Hanley,
Department of Bioengineering, University of California, Riverside, Riverside, California 92521, United States

Raviraj Vankayala,
Department of Bioengineering, University of California, Riverside, Riverside, California 92521, United States

Jenny T. Mac,
Department of Biochemistry, University of California, Riverside, Riverside, California 92521, United States

David D. Lo,
Department of Biomedical Sciences, University of California, Riverside, Riverside, California 92521, United States

Bahman Anvari
Department of Bioengineering, University of California, Riverside, Riverside, California 92521, United States

Abstract

Erythrocyte-derived particles activated by near-infrared (NIR) light present a platform for various phototheranostic applications. We have engineered such a platform with indocyanine green as the NIR-activated agent. A particular feature of these particles is that their diameters can be tuned from micro- to nanoscale, providing a potential capability for broad clinical utility ranging from vascular to cancer-related applications. An important issue related to clinical translation of these particles is their immunogenic effects. Herein, we have evaluated the early-induced innate immune response of these particles in healthy Swiss Webster mice following tail vein injection by measurements of specific cytokines in blood serum, the liver, and the spleen following euthanasia. In particular, we have investigated the effects of particle size and relative dose, time-dependent cytokine response for up to 6 h postinjection, functionalization of the nanosized particles with

Corresponding Author: **Bahman Anvari** – *Department of Bioengineering, University of California, Riverside, Riverside, California 92521, United States;* anvarib@ucr.edu.

Supporting Information

The Supporting Information is available free of charge at https://pubs.acs.org/doi/10.1021/acs.molpharma-ceut.0c00641. Characterization of NETs, quantification of endotoxin in ¼NETs and nNETs, representative bead clustering based on APC fluorescence emission, and representative 5-parameter logistic fits (PDF)

The authors declare the following competing financial interest(s): Author B.A. has a financial interest in Radoptics LLC, which is pursuing the commercial development of the particles reported in this manuscript. This interest did not interfere with the scientific work, judgement, or objectivity of any of the investigators with regards to the experimental procedures, analyses, reporting, and interpretation of results, or any other aspect of the study. All the remaining authors declare that they have no conflicts of interest.

Complete contact information is available at: https://pubs.acs.org/10.1021/acs.molpharmaceut.0c00641

folate or Herceptin, and dual injections of the particles 1 week apart. Mean concentrations of interleukin (IL)-6, IL-10, tumor necrosis factor (TNF)-α, and monocyte chemoattractant protein (MCP)-1 in response to injection of microsized particles at the investigated relative doses were significantly lower than the corresponding mean concentrations induced by lipopolysaccharide (positive control) at 2 h. All investigated doses of the nanosized particles induced significantly higher concentrations of MCP-1 in the liver and the spleen as compared to phosphate buffer saline (PBS) (negative control) at 2 h. In response to micro- and nanosized particles at the highest investigated dose, there were significantly higher levels of TNF-α in blood serum at 2 and 6 h postinjection as compared to the levels associated with PBS treatment at these times. Whereas the mean concentration of TNF-α in the liver significantly increased between 2 and 6 h postinjection in response to the injection of the microsized particles, it was significantly reduced during this time interval in response to the injection of the nanosized particles. In general, functionalization of the nanosized particles was associated with a reduction of IL-6 and MCP-1 in blood serum, the liver, and the spleen, and TNF-α in blood serum. With the exception of IL-10 in the spleen in response to nanosized particles, the second injection of micro- or nanosized particles did not lead to significantly higher concentrations of other cytokines at the investigated dose as compared to a single injection.

Graphical Abstract

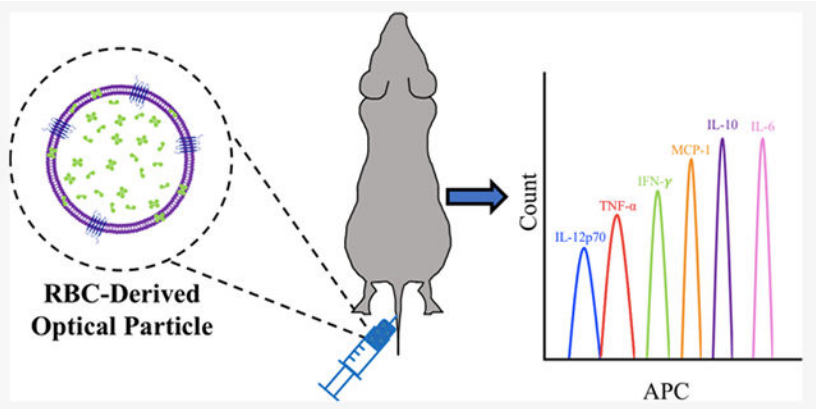

Keywords

cytokines; delivery systems; folate receptor; innate immune response; HER-2; red blood cells

INTRODUCTION

Use of near-infrared (NIR) light provides a capability for relatively deep biomedical optical imaging and phototherapy on the order of a few centimeters.[1,2] This increased depth of optical penetration results from minimal absorption and scattering by biological components over the NIR spectral band (≈700–2500 nm).[1,3] When combined with exogenous use of NIR fluorochromes, improved image contrast can be achieved as a result of reduced autofluorescence. To date, indocyanine green (ICG) remains as the only NIR fluorochrome

approved for use in humans by the United States Food and Drug Administration for specific clinical applications including retinal angiography[4] and assessment of liver function.[5]

Despite ICG's usage in both clinical procedures and investigational research,[6,7] ICG has a short half-life in plasma following intravascular administration (on the order of 3–4 min) with nearly exclusive uptake by hepatocytes and elimination from the body by the hepatobiliary mechanism.[8,9] Given the long circulation time of erythrocytes (on the order of 3-4 months) and their potential biocompatibility, they present an attractive platform for encapsulation of various cargos including ICG.[10–14] We reported the first results to encapsulate ICG into nanosized constructs derived from erythrocytes.[15] We refer to these constructs as NIR erythrocyte-derived transducers (NETs) because they can transduce the absorbed NIR light to emit fluorescence, generate heat, or mediate the production of reactive oxygen species.[16,17] We have also demonstrated that NETs can be functionalized with appropriate antibodies for targeted imaging of specific cell receptors.[18,19] Other investigators have also reported the use of erythrocyte-encapsulating ICG nanoparticles for light-mediated therapeutic applications.[20–23]

One feature of NETs is that their diameters can be tuned from micro- to nanosize via sonication or mechanical extrusion,[24] thereby providing a capability to develop a versatile platform for broad biomedical and clinical applications. Nanosized NETs (nNETs) (diameter < 200 nm) have relevance to tumor imaging and phototherapy via the enhanced permeability and retention effect.[25] Microsized NETs (μNETs) (diameter > 1 μm) have the potential for vascular imaging and photothermal treatment of cutaneous capillary malformations known as port wine stains.[17,26]

An important issue related to the use of NETs, as well as other erythrocyte-based delivery systems in clinical applications, is their potential immunogenic effects. Herein, we evaluate the early-induced innate immune response to μNETs and NNETs in healthy Swiss Webster (SW) mice following tail vein injection by measurements of specific cytokines in blood serum, the liver, and the spleen after euthanasia. In particular, during this acute phase, we investigate the effects of the particles' relative dose (relative number concentration) and time-dependent changes in the cytokine concentrations at 2, 4, and 6 h postinjection of the particles. We also evaluate the acute-phase immunogenicity of nNETs functionalized with folate or Herceptin as clinically relevant molecules that respectively target the folate receptor-α and human epidermal growth factor-2 (HER-2) on specific tumor types.[27–32] Finally, we investigate the immunogenic effects of dual injections administered one week apart.

MATERIALS AND METHODS

Fabrication of NETs.

Whole blood was drawn from healthy female SW mice using syringes coated in 2 mg/mL lithium heparin in nanopure water and stored in a flask containing ≈100 μL lithium heparin solution per 1 mL of mouse blood. Blood from ≈20 mice was drawn and pooled together to get a total volume of 20 mL of whole blood. Erythrocytes were separated from whole blood via centrifugation (≈2800g for 10 min at 4 °C). The plasma and buffy coat were removed,

and erythrocytes were washed in ≈320 mOsm phosphate buffered saline (PBS) (defined as 1× PBS) (Fisher Scientific). Erythrocytes were spun down (≈2800*g* for 10 min at 4 °C), the supernatant was removed, and the 1× PBS wash was repeated.

The intracellular hemoglobin of the erythrocytes was removed by hypotonic treatment. Specifically, erythrocytes were suspended in 0.25× PBS (≈80 mOsm) for ≈10 min at 4 °C and then centrifuged (≈31,000*g* for 20 min at 4 °C). After centrifugation, the hemoglobin-containing supernatant was discarded, and the erythrocytes were resuspended in 0.25× PBS. Hemoglobin depletion steps were repeated until the erythrocyte pellet was opaque, indicating the formation of erythrocyte ghosts (EGs). The pellet was then resuspended in 1× PBS.

To load ICG (MP Biomedicals) into EGs, 1 mL of EGs in 1× PBS was suspended in 1 mL of 0.1 M Sorenson's buffer (Na_2HPO_4/NaH_2PO_4, 140 mOsm, pH ≈ 8) and 1 mL of 75 μM ICG in nanopure water. The final concentration of ICG in the loading solution was 25 μM. The samples were allowed to incubate for ≈10 min at 4 °C, then centrifuged (≈56,000–70,000*g* for 1 h at 4 °C), and the supernatant removed. The pellet was resuspended in 1× PBS and centrifuged again (≈56,000*g* for 1 h at 4 °C). The supernatant was removed a final time, resulting in a μNET pellet, which was then resuspended in ≈ 1–1.5 mL of 1× PBS. We refer to this dose of μNET solution as 1× μNETs. To reduce the dose, 1× μNETs were diluted 1:1 with 1× PBS, resulting in 0.5× μNETs. Similarly, the 0.5× μNETs were diluted 1:1 with 1× PBS to get 0.25× μNETs. We note that because the lower doses of μNETs were diluted from the same solution of 1× μNETs, the relative protein and ICG content, as well as the number of particles would be scaled accordingly.

To fabricate nNETs, EGs were formed as described above and then diluted 1:10 in 1× PBS prior to an extrusion procedure. The diluted EGs were then extruded three times through 800 nm polycarbonate porous filters (Whatman) using a 10 mL automatic extruder (LIPEX Extruder, Evonik Canada Inc.). The resulting nanosized EGs (nEGs) were then centrifuged (≈70,000*g* for 1 h at 4 °C), and the supernatant was removed. The nEGs were resuspended in a volume of 1× PBS that was 10% of the volume of the supernatant removed, resulting in a 10:1 concentration ratio. The nEGs were then hypotonically loaded with ICG by adding 1 mL of nEG suspension in 1× PBS to 1 mL 0.1 M Sorenson's buffer and 1 mL 75 μM ICG in nanopure water as described above. The solution was then centrifuged and washed as described above, resulting in a nNET pellet, which was then resuspended in ≈ 1–1.5 mL of 1× PBS. We refer to this dose of nNET solution as 1× nNETs. To reduce the dose, 1× nNETs were diluted 1:1 with 1× PBS, resulting in 0.5× nNETs. Similarly, the 0.5× nNETs were diluted 1:1 with 1× PBS to get 0.25× nNETs. Similar to the μNETs, the relative protein and ICG content, as well as the number of particles would be scaled accordingly by diluting the 1× solution of nNETs.

Fabrication of Folate-Functionalized nNETs (FF-nNETs) and Herceptin-Functionalized nNETs (HF-nNETs).

To fabricate FF-nNETs, EGs were first prepared as described above. We then prepared a 5 mg/mL solution of 1,2-distearoyl-*sn*-glycero-3-phosphoethanolamine-*N*-[folate-(polyethylene glycol)] (DSPE-PEG-FOL) (2 kDa PEG, Nanosoft Polymers) in ≈100

°C nanopure water. The nanopure water was heated to fully dissolve the DPSE-PEG-FOL. We then incubated ≈200 μL of the DSPE-PEG-FOL solution with 1 mL of the EG suspension in 1× PBS for 30 min at room temperature, allowing the insertion of the DPSE component into the membrane of the EGs. This lipid-insertion method has also been reported for the functionalization of erythrocyte membrane-cloaked nanoparticles.[33] The DSPE-PEG-FOL-bearing EGs was then diluted 1:10 in 1× PBS and extruded as described above, resulting in DSPE-PEG-FOL-bearing nEGs. The DSPE-PEG-FOL-bearing nEGs was centrifuged (≈70,000*g* for 1 h at 4 °C), and the supernatant containing any excess DSPE-PEG-FOL was removed. The DSPE-PEG-FOL-bearing nEGs was then resuspended in a volume of 1× PBS equal to 10% the volume of the supernatant removed, resulting in a 10:1 concentration of the DSEP-PEG-FOL-bearing nEGs. The DSPE-PEG-FOL-bearing nEGs was then hypotonically loaded with ICG by adding 1 mL suspension of these particles in 1× PBS to 1 mL of 0.1 M Sorenson's buffer and 1 mL of 75 μM ICG in nanopure water as described above. The particles were then centrifuged and washed, as described above. The resulting FF-nNET pellet was resuspended in ≈ 1–1.5 mL 1× PBS. We refer to this dose of particles as 1× FF-nNETs.

To fabricate HF-nNETs, we used a methodology similar to our previous report in functionalizing nNETs with HER-2 antibodies.[18] We first prepared a 1 mg/100 μL Herceptin (gifted by Genentech) solution in nanopure water. Herceptin was oxidized by mixing 30 μL of the Herceptin solution with 20 μL of 100 mM sodium periodate ($NaIO_4$) (Acros Organics) in nanopure water and 50 μL 1× PBS. The solution was incubated at room temperature in the dark for 30 min. Excess oxidizing agent was removed by filtering the oxidized Herceptin through 100 kDa centrifugation filter tubes (Millipore Amicon) via centrifugation (≈3000*g* for 5 min at room temperature). The oxidized Herceptin was resuspended in 1× PBS, and the filtration step was repeated for a total of three spins. The oxidized Herceptin was then resuspended in 100 μL of 1× PBS.

To covalently attach the oxidized Herceptin to the surface of NETs, we used DSPE-PEG-amine (DSPE-PEG-NH_2) (2 kDa PEG, Nanocs Inc.) as a linker molecule. EGs in 1× PBS were prepared as described above and then incubated with 1 mg/mL of the DSPE-PEG-NH_2 lipid linker at room temperature for 30 min, resulting in lipid insertion of the DSPE component of the linker. The resulting DSPE-PEG-NH_2-bearing EGs were then diluted 1:10 in 1× PBS and extruded as described above. The resulting nanosized constructs were then hypotonically loaded with ICG by adding 1 mL suspension of these particles in 1× PBS to 1 mL of 0.1 M Sorenson's buffer, and 1 mL of 75 μM ICG in nanopure water as described above. The particles were then centrifuged as described above, and then resuspended in ≈150 μL of 1× PBS, resulting in DSPE-PEG-NH_2-bearing nNETs. The 100 μL of oxidized Herceptin was then add6ed to the ≈150 μL of DSPE-PEG-NH_2-bearing nNETs and allowed to incubate for 5 min at room temperature. The solution was then incubated with 10 μL of 20 mM sodium dithionite, as the reducing agent, for 1 h at 4 °C in the dark, resulting in covalent-coupling between the amine on the PEG lipid linker and the aldehyde on the oxidized Herceptin via reductive amination. The resulting HF-nNETs were washed in 1× PBS as described above, and then resuspended in ≈1–1.5 mL 1× PBS to produce 1× HF-nNETs.

In order to confirm functionalization with Herceptin, an aliquot of the HF-nNETs was also incubated with goat antihuman IgG fluorescein isothiocyanate (FITC)-labeled antibody (Southern Biotech) for 1 h at 4 °C in the dark and washed with 1× PBS as described above. The resulting solution was characterized as described below.

Characterization of Particles.

We used dynamic light scattering (DLS) (Zetasizer Nanoseries, NanoZS90, Malvern Instruments) to estimate the hydrodynamic diameters of all particles suspended in 1× PBS. For μNET measurements, we used a 1:20 dilution in 1× PBS of the 1× solution. For all other particles, we used a 1:40 dilution in 1× PBS of the 1× solutions to perform the DLS measurements. All measurements were made with the particle suspensions in polystyrene cuvettes with a 1 cm path length. Measurements were collected three times for each sample and used to determine the mean diameter and standard deviation (SD) for each sample population. For all other characterization measurements (i.e., zeta potentials and fluorescence spectra), we used a 1:80 dilution in 1× PBS of the 1× particle solutions, unless otherwise noted.

We measured the zeta potentials (Zetasizer Nanoseries, NanoZS90, Malvern Instruments) of the particles suspended in 1× PBS using folded capillary cells. Measurements were collected five times for each sample and used to determine the mean zeta potential and SD for each sample population.

We acquired the fluorescence spectra of all types of particles in response to photoexcitation at 720 ± 2.5 nm filtered from a 450 W xenon lamp using a fluorometer (Fluorolog-3 spectrofluorometer, Edison). We obtained the normalized wavelength (λ)-dependent fluorescence emission $\chi(\lambda)$ as follows

$$\chi(\lambda) = \frac{F(\lambda)}{1 - 10^{-A(\lambda_{ex})}} \quad (1)$$

where F is the fluorescence emission intensity in response to the excitation wavelength (λ_{ex}), and $A(\lambda_{ex})$ is the absorbance of the sample at λ_{ex}.

In order to confirm functionalization of the Herceptin, an aliquot of the 1× HF-nNETs was diluted 1:20 in 1× PBS, resulting in 0.05× HF-nNETs. Herceptin functionalization was confirmed by taking the fluorescence of 0.05× dose of the particles that were incubated with the FITC-labeled antibody in response to photoexcitation at 488 ± 2.5 nm and comparing it to the fluorescence of a 0.05× concentration of HF-nNETs not incubated with the antibody. The emission of both sets of particles was collected over the 508–750 nm spectral band. Characterization results are presented in Figure S1 (Supporting Information).

Further physical and optical characterization of nNETs and ¼NETs have been reported in our previous study[24] and are not repeated here. These characterizations included ICG loading efficiency, excitation-emission maps, relative fluorescence quantum yield as functions of ICG concentration, and the photostability of NETs. We have previously

provided the respective transmission and scanning electron microscopy images of nonfunctionalized nNETs and nNETs functionalized with HER-2 antibodies.[15,18]

Endotoxin Assessment.

To quantify the levels of endotoxin associated with μNETs and nNETs, we used the ToxinSensor chromogenic limulus amebocyte lysate (LAL) endotoxin assay kit (GenScript). μNETs and nNETs were prepared as described above. To ensure that there was no endotoxin contribution from the solvent (PBS), particles were suspended in LAL grade water after the last centrifugation. To retain the same relative amount of red blood cell (RBC) membranes in μNETs and nNETs, we diluted the respective particles by ≈30 and 12.5 times in LAL grade water so that the particles had similar absorbance values at 280 nm. Finally, μNETs and nNETs were diluted by 100 times in LAL grade water.

Once the μNETs and nNETs were prepared, we used the kit according to the instructions provided in the manufacturer's manual for endotoxin assessment. Using a spectrophotometer (Jasco-V670), we obtained the 545 nm absorbance values for three standard samples consisting of LAL grade water containing different known levels of endotoxin units (EU/mL), a blank LAL water grade standard without any endotoxin, the particles (μNETs and nNETs), and 0.5 mg/mL lipopolysaccharides (LPS) as the positive control. Absorbance of the blank sample at 545 nm was subtracted from the absorbance values of all other samples. Using the blank-subtracted absorbance values of the standards, we then generated a calibration curve relating the endotoxin levels to 545 nm absorbance values. Endotoxin levels of the μNET and nNET samples were subsequently determined from this calibration curve and are presented in Figure S2 (Supporting Information). The absorbance values of LPS were beyond the linear range of the kit because of their high endotoxin content.

Animal Studies.

Healthy female SW mice, 6–9 weeks old, (Taconic Biosciences) were used in all studies under a protocol approved by the University of California, Riverside Institutional Animal Care and Use Committee (protocol A-20170038). Animals were anesthetized by the inhalation of 2% isoflurane gas in oxygen. All animals received via tail vein a 100 μL injection of either 1× PBS (negative control), 0.5 mg/mL LPS (Sigma-Aldrich) in nanopure water (positive control), and various types of NET particles. The LPS had a manufacturer-reported potency of ≥500,000 EU/mg, which corresponds to ≥25,000 EU per mouse injection.

In Table 1, we provide a description of the various immunogenicity studies aimed at investigating the effects of particle dose (relative number concentration), time-dependent cytokine response at various times postinjection, functionalization, and dual injections set one week apart. Upon termination of a given study, mice were euthanized by inhalation of CO_2. The number of animals in each group for all studies was four. Following euthanasia, we collected the blood by cardiac puncture and extracted the liver and spleen, two organs associated with the reticuloendothelial system, for cytokine profiling. Blood was placed in BD Microtainer separator tubes (Becton, Dickinson and Company) and allowed to incubate on ice for 30–60 min before being centrifuged at ≈3400*g* for 15 min at 4 °C. The

supernatant was collected and stored at −80 °C. The livers and spleens were flash-frozen in liquid nitrogen and then stored at −80 °C.

For the organ analysis, all samples were thawed on ice at room temperature. Organs were weighed and then suspended in a volume of lysis buffer in μL equal to five times the organ weight in mg by following a modified version of the protocol by Amsen et al.[34] The lysis buffer was composed of 150 mM sodium chloride (NaCl), 1% Triton X-100, 5 mM ethyl-enediaminetetraacetic acid, 50 mM Tris-HCl, and ≈3.3 μL of Halt protease inhibitor cocktail (Fisher Scientific Company) per mL of lysis buffer. Following incubation in the lysis buffer for 5–20 min at room temperature, organs were homogenized using a tissue homogenizer (Omni TH 115, Omni International). The resulting solutions were placed on ice for at least an hour before being centrifuged at ≈3000*g* for 15 min at room temperature, and the supernatants were collected. Blood serum supernatants were allowed to thaw on ice at room temperature. The resulting supernatants for the organs and serum were then used for the analysis of various cytokines.

Cytokine Assessment.

A mouse inflammation BD cytometric bead array (CBA) kit (BD, Biosciences) was used to determine the cytokine concentrations in blood serum and homogenized organs. The kit was run according to the instructions in the manufacturer's manual. In brief, we first prepared a standard solution containing 5000 pg/mL each of interleukin (IL)-6, IL-10, tumor necrosis factor (TNF)-α, monocyte chemoattractant protein (MCP)-1, interferon-gamma (IFN-γ), and IL-12p70 by dissolving lyophilized standards provided by the kit in 2 mL of the assay diluent made of a buffered protein solution, according to the kit's manual. We chose to assay for these cytokines as they play important roles in inflammation.[35–37] The standard solution was serially diluted with the assay diluent to get standards with 2500, 1250, 625, 312, 156, 80, 40, and 20 pg/mL of each cytokine. The assay diluent was considered to be a standard without any cytokines. In each assay tube, we added 50 μL of assay capture beads (containing equal amounts of capture beads for IL-6, IL-10, TNF-α, MCP-1, IFN-γ, and IL-12p70), which would bind to the designated cytokine via specific capture antibodies for each cytokine. To each tube containing assay capture beads, we added either 50 μL of a cytokine standard, a blood serum sample, or a homogenized organ sample. Finally, we added 50 μL of mouse inflammation phycoerythrin (PE) detection reagent, which contains PE-conjugated antimouse antibodies for each of the cytokines, to all of the assay tubes. The PE served as the reporter molecule during the subsequent flow cytometry measurements. Solutions were allowed to incubate for 2 h at room temperature in the dark, during which time the capture beads and PE-conjugated antimouse antibodies would both bind to cytokines present in the sample. At the end of the incubation, 1 mL of wash buffer was added to each assay tube, followed by centrifugation for 5 min at 200*g* at 4 °C. We removed the supernatant and added 300 μL of wash buffer to each assay tube to resuspend the resulting pellet. The solution was then transferred to a flow cytometer tube.

Samples were analyzed using a BD LSR II flow cytometer equipped with 488 and 640 nm lasers. The instrument was set up according to BD's "guide to using BD FACSDiva software with BD CBA kits," and data were collected using the "Digital Instrument CBA Template"

for BD FACSDiva software. In brief, the voltages for forward scatter, side scatter, PE, and allophycocyanin (APC) fluorescence were set to 465–475, 190–200, 445–466, and 365–378 V, respectively. The exact voltages were determined using cytometer setup beads from the mouse inflammation BD CBA kit on the day of the assay. Once the voltages were set, data were recorded for each of the cytokine standards, followed by each of the samples.

Data were exported and analyzed using FCAP array according to BD Bioscience's "FCAP Array software version 3.0 User's Guide." In brief, the flow cytometry data were filtered of debris and clustered to form six distinct populations using histograms of the APC fluorescent signals, one for each of the beads that correspond to the six cytokines measured (Figure S3 in Supporting Information). The mean fluorescence intensity (MFI) of the PE fluorescent signal was measured for each population. The results from the standards for each experiment were fitted with a 5-parameter logistic curve, and the curve was used to correlate the MFI for each measurement to a concentration for the selected cytokine (Figure S4 in Supporting Information). This curve allowed us to extrapolate concentration values below the limit of detection of each cytokine and values above the maximum standard concentration of 5000 pg/mL. It is important to note, however, that MFI values above a certain value will correlate to the upper concentration limit of the 5-parameter logistic curve, resulting in some organ populations having the same concentration value for all four measurements. Populations with all the MFI values mapped to the same concentration value were handled as discussed below.

Data Analysis.

Concentrations for each flow cytometer measurement were analyzed using GraphPad Prism. In brief, all of the results for one experiment were grouped together. Outliers were detected using a Grubbs' test ($\alpha = 0.05$) and removed, resulting in some of the populations having $n = 3$ cytokine concentrations. The concentrations were then analyzed using Brown–Forsythe and Welch ANOVA tests. We used unpaired t-tests with Welch's correction to compare the mean of one population with the means of all other populations in that group. For populations where all of the MFI values were mapped to the same concentration value, the Welch ANOVA test could not be performed. Instead, we compared the mean of the population with other population means of interest using an unpaired t-test with Welch's correction. Unless otherwise noted, all of the unpaired t-tests with Welch's correction were two-tailed (see Table 1). In order to display the cytokine concentrations on a log 10 scale, concentration values equal to 0 were set to 0.05 pg/mL for graphical purposes. Statistical testing was done on the populations with the original 0 pg/mL concentration measurements. Finally, we used a F-test to compare the variances of two populations of interest, if needed. Statistical methods associated with each immunogenicity study are summarized in Table 1.

RESULTS

Effects of Particle Size and Dose.

The respective mean concentration values of IL-6 and TNF-α in blood serum at 2 h postinjection of 50 μg LPS were 20.37 and 2.86 ng/mL, respectively (Figure 1a,g). These values are comparable to the reported respective values of ≈12 ng/mL for IL-6 in blood

serum at 3 h and ≈13 ng/mL for TNF-α at 1 h postinjection of 50 μg LPS in C57B1/6/129-Ola mice by Berg et al.[38] As another example of validation, our estimated respective mean concentrations of 4.05 and 4.90 pg/mL for IL-6 in the liver and spleen, in response to PBS injection are also comparable to the reported mean baseline values of ≈18 pg/mL in the liver and ≈20 pg/mL in the spleen of C57BL/6 mice.[39]

Mean concentrations of IL-6, IL-10, TNF-α, and MCP-1 in response to μNETs were significantly lower than the mean concentration of these cytokines in response to LPS, regardless of μNET dose or the site of cytokines (blood serum, liver, spleen) (Figure 1a–c, d–f, g–i, and j–l, respectively). Levels of both IFN-γ and IL-12p70 induced by all doses of μNETs were not significantly different from the levels induced by PBS in blood serum, the liver, and the spleen (data not shown). While some of the μNETs doses did lead to significantly higher levels of the cytokines compared to the levels induced by PBS, there were no clear trends between the μNET dose and the significantly elevated cytokine levels. In addition, there were no significant differences between the induced cytokine levels for different μNET doses in the blood serum, liver, and spleen. Overall, these results show that while there were some increases in the mean concentrations of IL-6, IL-10, TNF-α, and MCP-1 relative to those induced by PBS, in general, they did not appear to correlate with the investigated μNET doses and are possibly due to variations among the response of the animals.

The levels of IL-12p70 induced by all investigated doses of nNETs were not significantly different from the levels induced by PBS in blood serum, the liver, and the spleen (data not shown). For IFN-γ, the levels induced by all doses of nNETs were not significantly different from those induced by PBS in blood serum and the liver. In the spleen, only the 0.5× nNETs induced a level of IFN-γ that was significantly higher than that induced by PBS. However, the [IFN-γ] induced by the 0.5× nNETs was still significantly lower than that induced by LPS, and the population mean concentration of IFN-γ induced by the 0.5× nNETs was only ≈3 pg/mL higher than that of PBS.

Mean IL-6 concentrations induced by all investigated doses of nNETs were significantly below the levels induced by LPS in blood serum, the liver, and the spleen (Figure 2a–c). In addition, a decrease in the nNET dose was associated with a decrease in the induced concentration of IL-6, indicating a dose response to the nNETs. Although the IL-6 concentrations induced by the nNETs were significantly lower than the levels induced by LPS for all investigated doses, administration of nNETs at all doses resulted in a statistically significant higher level of IL-6 in the liver as compared to PBS injection (Figure 2b). In addition, both the 1× and 0.5× doses resulted in statistically significant higher levels of IL-6 in the spleen (Figure 2c), and the 0.5× and 0.25× doses resulted in a statistically significant higher level of IL-6 in the blood serum as compared to PBS (Figure 2a). The variability in the response of animals may have been the reason that the higher concentrations of nNETs (1×) did not induce a statistically significant higher concentration of IL-6 in the blood serum.

The induced IL-10 mean concentration levels in response to all nNET doses were significantly lower than those associated with LPS in the blood serum and the spleen (Figure

2d,f); however, only the 1× dose of nNETs induced a significantly lower level of IL-10 in the liver compared to the levels induced by LPS (Figure 2e). In addition, there were no significant differences between the levels of IL-10 induced by PBS and any of the nNET doses in blood serum (Figure 2d). Only the 0.5× nNET dose resulted in significantly higher levels of IL-10 in the liver and spleen compared to PBS (Figure 2e,f). However, because there were no significant differences between the IL-10 levels induced by any of the other nNET doses, these results may be due to variability among the animal response rather than suggesting a dose-dependent IL-10 response.

Although all doses of nNETs induced significantly lower mean values of TNF-α compared to LPS in blood serum, the liver, and the spleen, there did appear to be some dose sensitivity (Figure 2g–i). Specifically, the 1× nNETs induced significantly higher mean concentration of TNF-α as compared to 0.5× nNETs, 0.25× nNETs, and PBS injections in blood serum, the liver, and the spleen. In addition, the 0.5× nNETs also induced a higher mean concentration of TNF-α than PBS in blood serum, the liver, and the spleen, while the 0.25× dose did not. These results suggest that higher doses of nNETs lead to higher concentrations of TNF-α; however, even the highest investigated dose of nNETs did not induce a TNF-α response comparable to that of LPS.

While the 1× nNETs did not induce a significantly lower mean concentration of MCP-1 in blood serum compared to LPS, it neither induced a significantly higher level compared to PBS (Figure 2j). Based on the results of the *F*-tests, the variances in MCP-1 induced concentrations in response to injection of LPS, and all doses of nNETs were significantly higher as compared to the variance associated with PBS injection in blood serum, the liver, and the spleen ($p < 0.05$). The variance in MCP-1 concentrations for the 1× nNETs in the blood serum was also significantly higher than the variances associated with injection of the other doses of nNETs ($p < 0.05$).

All doses of nNETs induced significantly higher mean concentrations of MCP-1 as compared to PBS in the liver and spleen. However, those levels were still significantly lower than the corresponding levels in response to LPS injection (Figure 2k,l). There was a dose-dependency effect where 1× nNETs injection resulted in a significantly higher mean concentration level of MCP-1 in the liver as compared to the 0.5× and 0.25× nNET injections (Figure 2k), and the 1× and 0.5× nNETs, resulting in higher MCP-1 concentrations in the spleen as compared to 0.25× nNETs (Figure 2l).

Time Dependency of Cytokine Response.

We used the 1× dose of μNETs and nNETs to investigate the dynamics of the induced concentration levels of IL-6, IL-10, TNF-α, and MCP-1 over a 6 h time interval following injection. We chose the 1× dose of NETs for this study because in general, it resulted in the greatest levels of the cytokines at 2 h postinjection for both μNETs and nNETs. IL-12p70 and IFN-γ were not investigated further because, for the most part, none of the investigated doses of μNETs and nNETs investigated resulted in significantly elevated concentrations of these two cytokines (data not shown).

For μNETs, the induced mean concentrations of IL-6, IL-10, TNF-α, and MCP-1 in blood serum did not significantly change over the time course of 2–6 h postinjection (Figure 3). When compared to the cytokine levels produced in response to PBS injection, only the TNF-α mean concentration levels induced by the μNETs were significantly higher at 2 and 6 h after injection (Figure 3c).

The response to the nNET injection was more varied among the animals. The only significant difference in the induced cytokine response was for TNF-α whose mean concentration was significantly higher at 2 h compared to 6 h postinjection ($p < 0.01$) (Figure 3c). Similar to the μNETs, the mean induced concentration of TNF-α in response to nNETs at 2 and 6 h postinjection were higher as compared to the levels induced by PBS injection (Figure 3c). None of the other cytokines had induced mean concentration levels that were significantly different from those of PBS at any of the investigated time points.

Mean values of μNET-induced concentrations of IL-6 and IL-10 in the liver at 2, 4, and 6 h postinjection were not significantly different from each other (Figure 4a,b). Although, the μNET-induced levels of IL-6 were only significantly higher than those in response to PBS at 4 and 6 h postinjection, IL-10 induced levels were not significantly different from PBS at any of the time points.

Induced mean concentrations of TNF-α at 4 and 6 h postinjection of μNETs, while not significantly different from each other, were significantly greater than the value at 2 h ($p < 0.05$) (Figure 4c). At 2 and 6 h postinjection, there were no significant differences between the mean concentration of TNF-α induced by the μNETs and the concentration induced by PBS, but at 4 h postinjection, the μNET-induced levels of TNF-α were significantly higher than the level induced by PBS. We observed a similar trend for the μNET-induced concentrations of MCP-1, where the mean values of the induced concentrations at 4 and 6 h were significantly higher than the mean concentration at 2 h ($p < 0.05$) (Figure 4d). In addition, while the MCP-1 concentration induced by the μNETs was significantly higher than the concentration induced by PBS for all three time points, they were still significantly lower than the concentrations induced by LPS for all three time points.

For the nNETs, we observed a similar trend for the induced cytokine dynamics in the liver. Specifically, there were no statistically significant differences between the concentrations of IL-6 and IL-10 induced by the various doses of nNETs at any of the time points (Figure 4a,b). Although, the mean concentration of nNET-induced IL-6 concentration at 4 h did not have a statistically significant higher value than those at 2 and 6 h, there was also a significantly higher variance in the measured concentration at 4 h as compared to those at 2 and 6 h ($p < 0.05$). The nNET-induced levels of IL-6 were only significantly higher than those induced by PBS 2 and 6 h postinjection. However, there were no significant differences between the nNET- and PBS-induced IL-10 levels at any of the time points.

Similar to the results shown in Figure 3, the wide range in IL-6, TNF-α, and MCP-1 concentration in the liver at 4 h is possibly because of the variability in response to nNET injection among the animals (Figure 4a,c,d). Mean concentrations of TNF-α and MCP-1 in the liver at 2 h were significantly higher than the corresponding concentrations at 6 h

postinjection (Figure 4c,d). However, the mean concentrations of these two cytokines at 4 h were not significantly different from those at 2 and 6 h. In addition, nNET-induced mean concentration of TNF-α and MCP-1 were only significantly higher than those in response to PBS at the 2 h postinjection time point.

In response to injection of 1× μNETs and 1× nNETs, there were no statistically significant changes in the induced concentrations of IL-6 and IL-10 in the spleen at 2, 4, and 6 h ($p > 0.05$) (Figure 5a,b). While there were no significant differences between the IL-10 levels induced by the μNETs and PBS at any of the time points, there were significantly higher levels of IL-6 at 2 and 6 h postinjection of μNETs as compared to PBS. There were no significant differences at 4 h postinjection between the IL-6 levels induced by PBS and the μNETs. Furthermore, the μNET-induced levels of IL-6 were significantly lower than the levels induced by LPS for all three time points.

For 1× μNETs, there were no significant differences in the mean concentration of TNF-α in the spleen at 2, 4, and 6 h ($p > 0.05$) (Figure 5c). In addition, there were no statistically significant differences between the TNF-α-induced concentrations by PBS and the μNETs at any of the time points. The 1× μNET-induced mean concentrations of MCP-1 in the spleen at 4 and 6 h were significantly higher than the mean concentration at 2 h ($p < 0.05$) (Figure 5d). Additionally, the MCP-1 concentrations induced by the μNETs were significantly higher than those by PBS for all three time points. However, the 1× μNET-induced mean concentrations of TNF-α and MCP-1 still remained significantly lower than the LPS-induced concentrations at all three measurement time points (Figure 5c,d).

Mean values of IL-6 and TNF-α concentrations in response to nNETs were only significantly higher at 2 h postinjection as compared to the respective values induced by PBS (Figure 5a,c). There were no statistically significant differences in the mean values of IL-10 in response to nNETs at any of the time points as compared to those in response to PBS (Figure 5b). Mean MCP-1 concentrations induced by the nNETs were significantly higher than those associated with PBS at 2 and 6 h postinjection, but not at 4 h postinjection (Figure 5d), possibly because of the variability of response among the animals injected with nNETs. Both TNF-α and MCP-1 mean concentration levels in the spleen at 6 h were significantly lower than their respective concentrations at 2 h (Figure 5c,d). However, the mean concentrations of these two cytokines at 4 h were not significantly different from their respective concentrations at 2 and 6 h.

Effects of nNET Functionalization with Folate or Herceptin.

We chose to investigate the effects of functionalization on the acute-phase response at 4 h postinjection of functionalized nNETs because at the 6 h time point, concentrations of TNF-α (Figures 3c, 4c, and 5c) had significantly decreased as compared to the 2 h time points. Based on the amounts of folate or Herceptin used in this study, there was a general trend in reduction of the induced IL-6 (Figure 6a–c) and MCP-1 (Figure 6j–l) concentrations in blood serum, the liver, and the spleen in response to injection of 1× FF-nNETs or 1× HF-nNETs as compared to the levels resulting from the injection of 1× nNETs. There was also a similar trend for IL-10 (Figure 6d) and TNF-α (Figure 6g) concentrations in blood serum following the injection of 1× FF-nNETs or 1× HF-nNETs.

Effect of Dual Injections of NETs One Week Apart.

Because the single 1× dose of the nNETs resulted in elevated levels of some of the investigated cytokines at 2 h postinjection, we aimed to investigate the effects of a dual injection of a lower dose (0.5×), which we had found to be less immunogenic (e.g., Figure 2l) when administered at a single dose. Overall, there were no statistically significant differences between the induced cytokine levels in response either to a single injection or dual injections one week apart either to 0.5× μNETs or 0.5× nNETs (Figure 7). The only exception was that there was a significantly higher concentration of IL-10 in the spleen after the second injection of the 0.5× nNETs (Figure 7f). We summarize our key findings associated with each of the immunogenic studies in Table 2.

DISCUSSION

We have focused our studies to the acute-phase of the innate immune response. For the effects of particle size and dose experiments, we chose to investigate the cytokine concentrations at 2 h postinjection because we were interested to know if the acute response could be elicited within a relatively short time period (e.g., 2 h). Cytokine (e.g., IL-6, TNF-α) expressions in response to LPS have been shown to peak in blood serum between 1 and 3 h.[38] We note that the initial phase of the innate response (prior to the acute-phase) is primarily due to the complement system of plasma proteins that act immediately to target the foreign materials (e.g., micro- and nanoparticles in blood) for direct lysis, or facilitating their phagocytosis or an inflammatory response by the sensor cells of the innate immune system.[40] Our findings that there were some cytokine activities suggest the continued innate response, requiring the involvement of cytokines to augment the actions of the complement system. Other examples of the interplay between the complement system activation and cytokine activity include C5a- and C3a-mediated production of TNF-α by macrophages[41,42] and the reciprocal action of proinflammatory cytokines in amplification of complement system activity.[43]

Macrophages and neutrophils are major inflammatory sensor cells equipped with innate pattern recognition receptors that stimulate phagocytic responses to engulf and destroy foreign materials. Whereas neutrophils extravasate out of the blood vessels to enter an inflamed tissue, macrophages reside in almost all tissues and are particularly found in key filtration organs, such as the liver, spleen, and the lungs, where they perform phagocytic functions.[44] In our previous study, we found that about 20, and 5% of administered μNETs were found in the spleen and liver of healthy SW mice at 6 h post-tail vein injection, respectively.[45] For nNETs, the respective percentages in the spleen and liver were about 25 and 13% at 6 h post-tail vein injection. Spleen is the filtration organ involved in removal of senescent or damaged RBCs from circulation by resident macrophages.[46] Hence, in this study, we particularly assayed for the presence of cytokines in the spleen and liver.

Phagocytic sensor cells can also secrete cytokines, small proteins (about 25 kDa), to mediate an inflammatory response. Cytokines can either act as synergists or antagonists with one another[47–49] and are considered as some of the biomarkers in assessing the immunogenicity of various nanoparticles.[47] They can act as proinflammatory cytokines, which lead to an

immune response, or as anti-inflammatory cytokines to counteract and control inflammation responses.[49,50]

IL-6 is a pleiotropic cytokine with both pro- and anti-inflammatory roles, promptly produced by various cells such as endothelial cells, monocytes, mesenchymal cells, and immune cells including macrophages.[49,51] In the initial stages of an inflammatory response, it moves from the bloodstream to the liver where it acts on hepatocytes to synthesize and secrete acute-phase proteins with broad specificity for pathogen-associated molecular patterns into blood.[52] Our results show that as early as 2 h post-tail vein injection of μNETs and nNETs, IL-6 levels in general were elevated and in some cases, significantly higher than the levels induced by PBS injection (although still at significantly lower levels than those induced by LPS) (Figures 1a–c and 2a–c). Elevated levels of IL-6 in blood serum may have been due to production by monocytes.[51] Mean concentrations of IL-6 in blood serum, the liver, and the spleen at 6 h were not significantly different than those at 2 h postinjection of either 1× μNETs or 1× nNETs (Figures 3a, 4a, and 5a).

TNF-α is a proinflammatory cytokine produced by activated macrophages.[48,53] It has a range of biological activities and is also involved in the initiation of the acute-phase response. TNF-α is a potent activator of endothelial cells, causing expression of blood clotting proteins and increased vascular permeability. There was a dose-dependency effect where 1× nNETs induced a significantly higher concentration of TNF-α as compared to 0.5× nNETs and 0.25× nNETs in blood serum, the liver, and the spleen at 2 h postinjection (Figure 2g–i). At 6 h postinjection of 1× nNETs, mean concentrations of TNF-α became significantly lower in blood serum, the liver, and the spleen as compared to the respective mean concentrations at 2 h (Figures 3c, 4c, and 5c).

IL-10 is a potent anti-inflammatory cytokine that can be produced by various cell types including monocytes, macrophages, and dendritic cells (DCs).[48,49,54] Its main effects are to suppress macrophage and DC functions by deactivating their cytokine synthesis.[49,54 56] In general, the μNET- and nNET-induced levels of IL-10 were not significantly different from those induced by PBS in blood serum, the liver, and the spleen (Figures 1d–f and 2d–f, respectively). In addition, mean concentrations of IL-10 in blood serum, the liver, and the spleen did not change significantly when comparing any of the time points postinjection of either 1× μNETs or 1× nNETs (Figures 3b, 4b, and 5b).

Chemokines are chemoattractant cytokines released during the earliest phases of infection, inducing directed chemotaxis of neutrophils, monocytes, and other effector cells of innate immunity from blood into sites of infection.[57] MCP-1 (also designated as CCL2) is a member of the CC group of chemokines produced by a variety of cell types including fibroblasts and endothelial cells, but with monocytes and macrophages as the primary sources.[35,58] It is a potent attractant of monocytes, inducing their migration from the bloodstream to become tissue macrophages.[35,59] There was a general trend that injection of μNETs and nNETs at 1× dose led to elevated levels of MCP-1 as early as 2 h post-tail vein injection (Figures 1j–l and 2j–l). Additionally, all investigated doses of nNETs induced significantly higher concentrations of MCP-1 in the liver and spleen as compared to PBS (Figure 2k,l). While the mean concentration of MCP-1 in the spleen at 6 h postinjection of

1× μNETs was significantly higher than its respective concentrations at 2 h, the trend was reversed in response to injection of 1× nNETs (Figure 5d).

Overall, it appears that nNETs were associated with higher induced concentrations of IL-6, TNF-α, and MCP-1 (Figures 1 and 2) as compared to those induced by μNETs. Because μNETs and nNETs had similar zeta potentials, it is unlikely that the zeta potential had a major role in modulating the immune response to μNETs and nNETs. It has been suggested that the toxicity of nanoparticles can result from their increased surface-to-volume ratio, giving rise to a greater proportion of reactive surface molecules to be displayed on the surface compared to interior molecules.[60] Consistent with this explanation, nNETs would present a larger fraction of potentially immunogenic surface molecules that can be recognized by the inflammatory sensor cells. In addition, conformational changes to some of the immunomodulatory surface proteins during the fabrication process of nNETs (e.g., formed by extrusion of microsized EGs) may result in our observed cytokine levels. For example, CD47, a transmembrane glycoprotein on RBCs, impedes phagocytosis through an inhibitory interaction with the signal-regulatory protein-alpha (SIRP-α) expressed on macrophages of the reticuloendothelial system.[61,62] However, conformational changes in CD47 can switch its role from an inhibitory to an activating molecule, leading to phagocytosis of RBCs.[63] It is possible that mechanically induced conformation changes to CD47 (e.g., through mechanical extrusion of EGs) would lead to a more efficient phagocytosis of nNETs and possibly enhanced secretion of specific cytokines by phagocytic sensor cells.

There was a general trend in reduction of IL-6, TNF-α, and MCP-1 by functionalizing the nNETs with folate or Herceptin (Figure 6). Our functionalization method involved the use of a DSPE-PEG linker inserted into the lipid phase of the particles. Abrams et al. reported that several cytokines including IL-6 and TNF-α were released into the plasma of mice in which lipid nanoparticles were administered.[64] It is possible that functionalization of nNETs based on DSPE-PEG lipid insertion was effective in camouflaging the lipid phase of the particles from recognition by the inflammatory sensor cells to ultimately reduce the released levels of IL-6, TNF-α, and MCP-1. It is also possible that the detection capability of the inflammatory sensor cells were reduced because of induced steric hindrance effects resulting from the presence of folate or Herceptin conjugated onto nNETs.

The second injection of either μNETs or nNETs at 0.5×, one week after their respective first injection, in some cases, resulted in elevation of some of the cytokines, although the differences were not statistically significant ($p > 0.05$) (Figure 7) (with the exception of IL-10 in the spleen after the second injection of 0.5× nNETs). Despite this finding, the role of the adaptive immune system in generating immunological memory needs to be investigated.

Other researchers have also investigated the immunogenicity of erythrocyte-based constructs. For example, Luk et al. have reported that injection of RBC-cloaked nanoparticles loaded with doxorubicin in C57BL/6 mice did not result in a significant increase in levels of IL-6 in blood serum 6 h postinjection.[65] He el al show that injection of two-dimensional $MoSe_2$ nanosheets camouflaged with RBC membranes did not induce

elevated levels of IL-6, IL-12, or TNF-α in the serum of SD mice 24–72 h postinjection compared to mice injected with saline.[66] Similarly, Sun et al. report that chlorin e6 imbedded erythrocyte membrane vesicles containing Prussian blue nanoparticles did not induce elevated levels of TNF-α in the blood serum of KM mice 1–7 days postinjection as compared to the PBS control group.[67] While our results indicate some elevated levels of inflammatory cytokines during the acute phase (studies over 2–6 h), these other studies suggest that any cytokine elevation due to RBC-derived constructs would return to baseline levels within 24 h and remain stable for up to 7 days postinjection.

Because our endotoxin assessment of μNETs and nNETs showed some endotoxic activity above those for the standard samples (Figure S2), it is possible that the elevations in some of the cytokine level measurements may have a component because of endotoxins, possibly introduced during the fabrication process. If this is the case, then some of the measured cytokine levels may actually overestimate the acute-phase response. In some cases, the mean cytokine (TNF-α) levels due to 0.5× and 0.25× ¼NETs (Figure 1g) and 0.25× nNETs (Figure 2g) were not significantly different those that induced by PBS, and comparable to the reported value of ≈68 pg/mL reported by Sun et al.,[67] indicating the absence of an immune response due to NET-based endotoxicity. Nevertheless, it is important that for ultimate clinical translation, the processes for particles fabrication and quality control are made in compliance with good manufacturing practice guidelines.

While cytokines are important biomarkers in evaluating the immunogenicity of particle-based delivery systems such as NETs, additional biomarkers for comprehensive immunotoxicity evaluation include blood chemistry, hematology, and histology.[68] Our results from a previous study show that the levels of biomarker enzymes alanine aminotransferase and aspartate aminotransferase, associated with the liver, and creatinine and urea nitrogen, associated with kidney functions were not altered in a statistically significant manner at 24 h postinjection of ¼NETs or nNETs in healthy SW mice.[45] Values of RBC count, mean corpuscular volume, hemoglobin, and % hematocrit were not altered in response to injection of ¼NETs or nNETs. Similarly, histological sections of the liver, spleen, lung, heart, and kidney did not show any pathological alterations. These results are consistent with those reported by Luk et al. where RBC count, platelet count, hemoglobin, and % hematocrit were not significantly different from those of mice injected with a sucrose solution[65] and those by Rao et al., where the nanoparticles did not induce hepatic or renal toxicity.[69] While in this study, we have focused on the acute phase of the innate immune response, understanding of the complete immune response including the roles of the complement system and the adaptive immune response in generating long-term immunological memory associated with repeated administration of these particles, and the interplay between innate and adaptive immunity are needed.

CONCLUSIONS

We have evaluated the acute phase of the innate immune response to NETs in healthy SW mice following tail vein injection. In particular, we found that both 1× ËNETs and 1× nNETs resulted in statistically significant higher levels of TNF-α in blood serum at 2 and 6 h postinjection as compared to the levels associated with PBS treatment at these times.

Cytokine response to 1× nNETs at 2 h also included significantly higher levels of IL-6 in the liver and spleen, TNF-α in blood serum, the liver, and the spleen, and MCP-1 in the liver and spleen as compared to PBS-induced levels. Functionalization of nNETs with folate or Herceptin was associated with a general trend in reduction of IL-6 and MCP-1 concentrations in blood serum, the liver, and the spleen, and TNF-α and IL-10 concentration reduction in blood serum. With the exception of IL-10 in the spleen in response to nNETs, the second injection of ¼NETs and nNETs at 0.5× did not lead to significantly higher concentrations of other cytokines as compared to a single injection. Future studies are needed to evaluate the roles of the complement system and adaptive immunity in response to these particles.

Supplementary Material

Refer to Web version on PubMed Central for supplementary material.

ACKNOWLEDGMENTS

The authors would like to thank Dr. Meera Nair and Dr. Jiang Li for their help in obtaining the flow cytometry measurements using the LSRII flow cytometer.

Funding

This study was supported in part by a grant for the National Institute of Arthritis and Musculoskeletal and Skin Diseases (R01-AR068067).

REFERENCES

(1). Frangioni J. In vivo near-infrared fluorescence imaging. Curr. Opin. Chem. Biol 2003, 7, 626–634. [PubMed: 14580568]

(2). Hong G; Antaris AL; Dai H Near-infrared fluorophores for biomedical imaging. Nat. Biomed. Eng 2017, 1, 0010.

(3). Weissleder R. A clearer vision for in vivo imaging. Nat. Biotechnol 2001, 19, 316–317. [PubMed: 11283581]

(4). Yannuzzi LA Indocyanine green angiography: a perspective on use in the clinical setting. Am. J. Ophthalmol 2011, 151, 745–751.e1. [PubMed: 21501704]

(5). Vos JJ; Wietasch JKG; Absalom AR; Hendriks HGD; Scheeren TWL Green light for liver function monitoring using indocyanine green? An overview of current clinical applications. Anaesthesia 2014, 69, 1364–1376. [PubMed: 24894115]

(6). Veys I; Pop C-F; Barbieux R; Moreau M; Noterman D; De Neubourg F; Nogaret J-M; Liberale G; Larsimont D; Bourgeois P ICG fluorescence imaging as a new tool for optimization of pathological evaluation in breast cancer tumors after neoadjuvant chemotherapy. PLoS One 2018, 13, No. e0197857.

(7). Nagahara R; Onda N; Yamashita S; Kojima M; Inohana M; Eguchi A; Nakamura M; Matsumoto S; Yoshida T; Shibutani M Fluorescence tumor imaging by i.v. administered indocyanine green in a mouse model of colitis-associated colon cancer. Cancer Sci. 2018, 109, 1638–1647. [PubMed: 29520973]

(8). Cowan V. Evaluation of Liver Function. In Liver Anesthesiology and Critical Care Medicine; Wagener G, Ed.; Springer Berlin Heidelberg: New York, NY, 2018; pp 79–85.

(9). De Gasperi A; Mazza E; Prosperi M Indocyanine green kinetics to assess liver function: ready for a clinical dynamic assessment in major liver surgery? World J. Hepatol 2016, 8, 355–367. [PubMed: 26981173]

(10). Hamidi M; Zarrin A; Foroozesh M; Mohammadi-Samani S Applications of carrier erythrocytes in delivery of biopharmaceuticals. J. Controlled Release 2007, 118, 145–160.

(11). Muzykantov VR Drug delivery by red blood cells: vascular carriers designed by Mother Nature. Expet Opin. Drug Deliv 2010, 7, 403–427.

(12). Yoo J-W; Irvine DJ; Discher DE; Mitragotri S Bioinspired, bioengineered and biomimetic drug delivery carriers. Nat. Rev. Drug Discovery 2011, 10, 521–535. [PubMed: 21720407]

(13). Hu C-MJ; Fang RH; Zhang L Erythrocyte-inspired delivery systems. Adv. Healthcare Mater 2012, 1, 537–547.

(14). Villa CH; Anselmo AC; Mitragotri S; Muzykantov V Red blood cells: supercarriers for drugs, biologicals, and nanoparticles and inspiration for advanced delivery systems. Adv. Drug Delivery Rev 2016, 106, 88–103.

(15). Bahmani B; Bacon D; Anvari B Erythrocyte-derived phototheranostic agents: hybrid nano-vesicles containing indocyanine green for near infrared imaging and therapeutic applications. Sci. Rep 2013, 3, 2180. [PubMed: 23846447]

(16). Burns JM; Vankayala R; Mac JT; Anvari B Erythrocyte-derived theranostic nanoplatforms for near infrared fluorescence imaging and photodestruction of tumors. ACS Appl. Mater. Interfaces 2018, 10, 27621–27630. [PubMed: 30036031]

(17). Jia W; Burns JM; Villantay B; Tang JC; Vankayala R; Lertsakdadet B; Choi B; Nelson JS; Anvari B Intravital vascular phototheranostics and real-time circulation dynamics of micro- and nanosized erythrocyte-derived carriers. ACS Appl. Mater. Interfaces 2020, 12, 275–287. [PubMed: 31820920]

(18). Mac JT; Nuñez V; Burns JM; Guerrero YA; Vullev VI; Anvari B Erythrocyte-derived nano-probes functionalized with antibodies for targeted near infrared fluorescence imaging of cancer cells. Biomed. Opt. Express 2016, 7, 1311–1322. [PubMed: 27446657]

(19). Hanley T; Yin R; Mac JT; Tan W; Anvari B Functionalized erythrocyte-derived optical nanoparticles to target ephrin-b2 ligands. J. Biomed. Opt 2019, 24, 1–9.

(20). Hui L; Qin S; Yang L Upper critical solution temperature polymer, photothermal agent, and erythrocyte membrane coating: an unexplored recipe for making drug carriers with spatiotemporally controlled cargo release. ACS Biomater. Sci. Eng 2016, 2, 2127–2132. [PubMed: 33465888]

(21). Sun X; Wang C; Gao M; Hu A; Liu Z Remotely controlled red blood cell carriers for cancer targeting and near-infrared light-triggered drug release in combined photothermal–chemotherapy. Adv. Funct. Mater 2015, 25, 2386–2394.

(22). Ren H; Liu J; Li Y; Wang H; Ge S; Yuan A; Hu Y; Wu JOxygen self-enriched nanoparticles functionalized with erythrocyte membranes for long circulation and enhanced phototherapy. Acta Biomater. 2017, 59, 269–282. [PubMed: 28663143]

(23). Wang P; Wang X; Luo Q; Li Y; Lin X; Fan L; Zhang Y; Liu J; Liu X Fabrication of red blood cell-based multimodal theranostic probes for second near-infrared window fluorescence imaging-guided tumor surgery and photodynamic therapy. Theranostics 2019, 9, 369–380. [PubMed: 30809280]

(24). Tang JC; Partono A; Anvari B Near-infrared-fluorescent erythrocyte-mimicking particles: physical and optical characteristics. IEEE Trans. Biomed. Eng 2019, 66, 1034–1044. [PubMed: 30130175]

(25). Peer D; Karp JM; Hong S; Farokhzad OC; Margalit R; Langer R Nanocarriers as an emerging platform for cancer therapy. Nat. Nanotechnol 2007, 2, 751–760. [PubMed: 18654426]

(26). Burns JM; Jia W; Nelson JS; Majaron B; Anvari B Photothermal treatment of port-wine stains using erythrocyte-derived particles doped with indocyanine green: a theoretical study. J. Biomed. Opt 2018, 23, 1–10.

(27). Leamon CP; Low PS Folate-mediated targeting: from diagnostics to drug and gene delivery. Drug Discovery Today 2001, 6, 44–51. [PubMed: 11165172]

(28). Siegel BA; Dehdashti F; Mutch DG; Podoloff DA; Wendt R; Sutton GP; Burt RW; Ellis PR; Mathias CJ; Green MA; Gershenson DM Evaluation of ^{111}In-DTPA-folate as a receptor-targeted diagnostic agent for ovarian cancer: initial clinical results. J. Nucl. Med 2003, 44, 700–707. [PubMed: 12732670]

(29). Teng L; Xie J; Teng L; Lee RJ Clinical translation of folate receptor-targeted therapeutics. Expet Opin. Drug Deliv 2012, 9, 901–908.

(30). Vergote IB; Marth C; Coleman RL Role of the folate receptor in ovarian cancer treatment: evidence, mechanism, and clinical implications. Cancer Metastasis Rev. 2015, 34, 41–52. [PubMed: 25564455]

(31). Moasser MM Targeting the function of the HER2 oncogene in human cancer therapeutics. Oncogene 2007, 26, 6577–6592. [PubMed: 17486079]

(32). Gutierrez C; Schiff R HER2: biology, detection, and clinical implications. Arch. Pathol. Lab. Med 2011, 135, 55–62. [PubMed: 21204711]

(33). Fang RH; Hu C-MJ; Chen KNH; Luk BT; Carpenter CW; Gao W; Li S; Zhang D-E; Lu W; Zhang L Lipid-insertion enables targeting functionalization of erythrocyte membrane-cloaked nanoparticles. Nanoscale 2013, 5, 8884–8888. [PubMed: 23907698]

(34). Amsen D; Visser KE; Town T Approaches to determine expression of inflammatory cytokines. Methods Mol. Biol 2009, 511, 107–142. [PubMed: 19347295]

(35). Deshmane SL; Kremlev S; Amini S; Sawaya BE Monocyte chemoattractant protein-1 (MCP-1): an overview. J. Interferon Cytokine Res 2009, 29, 313–326. [PubMed: 19441883]

(36). Gee K; Guzzo C; Che Mat N; Ma W; Kumar A The IL-12 family of cytokines in infection, inflammation and autoimmune disorders. Inflammation Allergy: Drug Targets 2009, 8, 40–52. [PubMed: 19275692]

(37). Chen L; Deng H; Cui H; Fang J; Zuo Z; Deng J; Li Y; Wang X; Zhao L Inflammatory responses and inflammation-associated diseases in organs. Oncotarget 2017, 9, 7204–7218. [PubMed: 29467962]

(38). Berg DJ; Kühn R; Rajewsky K; Müller W; Menon S; Davidson N; Grünig G; Rennick D Interleukin-10 is a central regulator of the response to LPS in murine models of endotoxic shock and the Shwartzman reaction but not endotoxin tolerance. J. Clin. Invest 1995, 96, 2339–2347. [PubMed: 7593621]

(39). Ren J; Ding Y; Yu H; Zhou Y; Yu W Effects on the expression of pro-inflammatory cytokines in the liver and spleen after oral administration of Porphyromonas gingivalis in mice. Biomed. Res 2018, 29, 1603–1609.

(40). Moghimi SM; Andersen AJ; Ahmadvand D; Wibroe PP; Andresen TL; Hunter AC Material properties in complement activation. Adv. Drug Delivery Rev 2011, 63, 1000–1007.

(41). Markiewski MM; Lambris JD The role of complement in inflammatory diseases from behind the scenes into the spotlight. Am. J. Pathol 2007, 171, 715–727. [PubMed: 17640961]

(42). Takabayashi T; Vannier E; Clark BD; Margolis NH; Dinarello CA; Burke JF; Gelfand JA A new biologic role for C3a and C3a desArg: regulation of TNF-alpha and IL-1 beta synthesis. J. Immunol 1996, 156, 3455–3460. [PubMed: 8617973]

(43). Mäck C; Jungermann K; Götze O; Schieferdecker HL Anaphylatoxin C5a actions in rat liver: synergistic enhancement by C5a of lipopolysaccharide-dependent a_2-macroglobulin gene expression in hepatocytes via IL-6 release from Kupffer cells. J. Immunol 2001, 167, 3972–3979. [PubMed: 11564816]

(44). Gustafson HH; Holt-Casper D; Grainger DW; Ghandehari H Nanoparticle uptake: the phagocyte problem. Nano Today 2015, 10, 487–510. [PubMed: 26640510]

(45). Vankayala R; Mac JT; Burns JM; Dunn E; Carroll S; Bahena EM; Patel DK; Griffey S; Anvari B Biodistribution and toxicological evaluation of micron- and nano-sized erythrocyte-derived optical particles in healthy Swiss Webster mice. Biomater. Sci 2019, 7, 2123–2133. [PubMed: 30869663]

(46). Mebius RE; Kraal G Structure and function of the spleen. Nat. Rev. Immunol 2005, 5, 606–616. [PubMed: 16056254]

(47). Elsabahy M; Wooley KL Cytokines as biomarkers of nanoparticle immunotoxicity. Chem. Soc. Rev 2013, 42, 5552–5576. [PubMed: 23549679]

(48). Parkin J; Cohen B An overview of the immune system. Lancet 2001, 357, 1777–1789. [PubMed: 11403834]

(49). Opal SM; DePalo VA Anti-Inflammatory Cytokines. Chest 2000, 117, 1162–1172. [PubMed: 10767254]

(50). Dinarello CA Proinflammatory cytokines. Chest 2000, 118, 503–508. [PubMed: 10936147]

(51). Seshadri S; Kannan Y; Mitra S; Parker-Barnes J; Wewers MD MAIL Regulates human monocyte IL-6 production. J. Immunol 2009 183, 5358–5368. [PubMed: 19783680]

(52). Tanaka T; Narazaki M; Kishimoto T IL-6 in inflammation, immunity, and disease. Cold Spring Harbor Perspect. Biol 2014, 6, a016295.

(53). Wang X; Lin Y Tumor necrosis factor and cancer, buddies or foes? Acta Pharmacol. Sin 2008, 29, 1275–1288. [PubMed: 18954521]

(54). Couper KN; Blount DG; Riley EM IL-10: the master regulator of immunity to infection. J. Immunol 2008, 180, 5771–5777. [PubMed: 18424693]

(55). Brandtzaeg P; Osnes L; Ovstebø R; Joø GB; Westvik AB; Kierulf P Net inflammatory capacity of human septic shock plasma evaluated by a monocyte-based target cell assay: identification of interleukin-10 as a major functional deactivator of human monocytes. J. Exp. Med 1996, 184, 51–60. [PubMed: 8691149]

(56). Clarke CJP; Hales A; Hunt A; Foxwell BMJ IL-10-mediated suppression of TNF-α production is independent of its ability to inhibit NFκB activity. Eur. J. Immunol 1998, 28, 1719–1726. [PubMed: 9603479]

(57). Luster AD The role of chemokines in linking innate and adaptive immunity. Curr. Opin. Immunol 2002, 14, 129–135. [PubMed: 11790543]

(58). Matsukawa A; Hogaboam CM; Lukacs NW; Kunkel SL Chemokines and innate immunity. Rev. Immunogenet 2000, 2, 339–358. [PubMed: 11256744]

(59). Charo IF; Ransohoff RM The many roles of chemokines and chemokine receptors in inflammation. N. Engl. J. Med 2006, 354, 610–621. [PubMed: 16467548]

(60). Nel A; Xia T; Mädler L; Li N Toxic potential of materials at the nanolevel. Science 2006, 311, 622–627. [PubMed: 16456071]

(61). Oldenborg P-A; Gresham HD; Lindberg FP CD47-signal regulatory protein α (SIRPα) regulates Fγ and complement receptor–mediated phagocytosis. J. Exp. Med 2001, 193, 855–861. [PubMed: 11283158]

(62). Oldenborg P-A; Zheleznyak A; Fang Y-F; Lagenaur CF; Gresham HD; Lindberg FP Role of CD47 as a marker of self on red blood cells. Science 2000, 288, 2051–2054. [PubMed: 10856220]

(63). Burger P; Hilarius-Stokman P; de Korte D; van den Berg TK; van Bruggen R CD47 functions as a molecular switch for erythrocyte phagocytosis. Blood 2012, 119, 5512–5521. [PubMed: 22427202]

(64). Abrams MT; Koser ML; Seitzer J; Williams SC; DiPietro MA; Wang W; Shaw AW; Mao X; Jadhav V; Davide JP; Burke PA; Sachs AB; Stirdivant SM; Sepp-Lorenzino L Evaluation of efficacy, biodistribution, and inflammation for a potent SiRNA nanoparticle: effect of dexamethasone co-treatment. Mol. Ther 2010 18, 171–180. [PubMed: 19738601]

(65). Luk BT; Fang RH; Hu C-MJ; Copp JA; Thamphiwatana S; Dehaini D; Gao W; Zhang K; Li S; Zhang L Safe and immunocompatible nanocarriers cloaked in RBC membranes for drug delivery to treat solid tumors. Theranostics 2016, 6, 1004–1011. [PubMed: 27217833]

(66). He L; Nie T; Xia X; Liu T; Huang Y; Wang X; Chen T Designing bioinspired 2D MoSe2 nanosheet for efficient photothermal-triggered cancer immunotherapy with reprogramming tumor-associated macrophages. Adv. Funct. Mater 2019, 29, 1901240.

(67). Sun L; Li Q; Hou M; Gao Y; Yang R; Zhang L; Xu Z; Kang Y; Xue P Light-activatable Chlorin e6 (Ce6)-imbedded erythrocyte membrane vesicles camouflaged Prussian blue nanoparticles for synergistic photothermal and photodynamic therapies of cancer. Biomater. Sci 2018, 6, 2881–2895. [PubMed: 30192355]

(68). Dobrovolskaia MA; McNeil SE Immunological properties of engineered nanomaterials. Nat. Nanotechnol 2007, 2, 469–478. [PubMed: 18654343]

(69). Rao L; Bu L-L; Xu J-H; Cai B; Yu G-T; Yu X; He Z; Huang Q; Li A; Guo S-S; Zhang W-F; Liu W; Sun Z-J; Wang H; Wang T-H; Zhao X-Z Red blood cell membrane as a biomimetic nanocoating for prolonged circulation time and reduced accelerated blood clearance. Small 2015, 11, 6225–6236. [PubMed: 26488923]

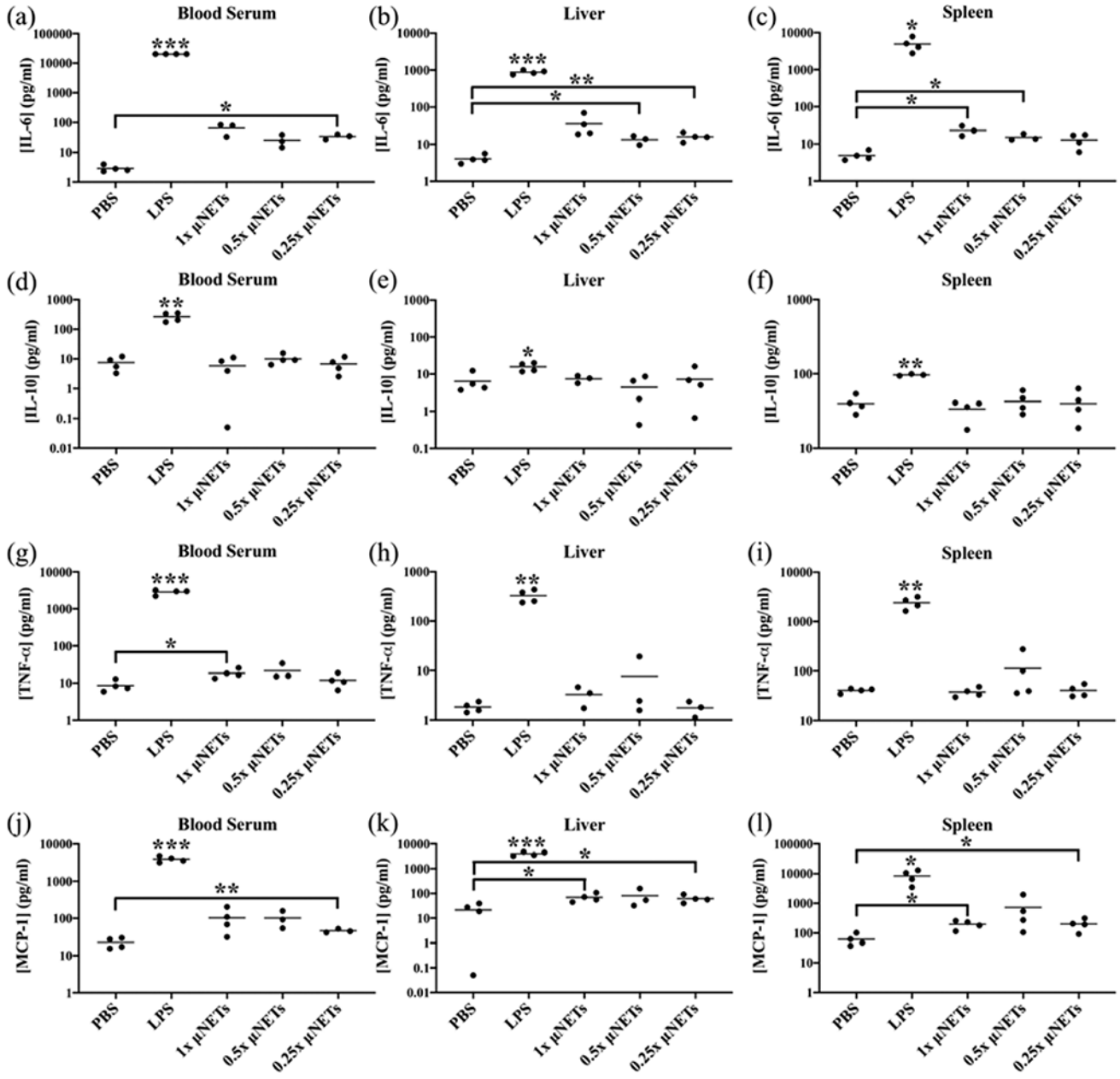

Figure 1.

Effects of μNET dose on cytokine production at 2 h post-tail vein injection. Concentration measurements (as represented by dots) for (a–c) IL-6, (d–f) IL-10, (g–i) TNF-α, and (j–l) MCP-1 in the blood serum, liver, and spleen, respectively, are shown with the population mean (horizontal bars). PBS and LPS correspond to negative and positive controls, respectively. Statistical significance of * ($p < 0.05$), ** ($p < 0.01$), and ***($p < 0.001$) are indicated. Significance markings directly above LPS indicate that the measured cytokines in response to LPS injection are significantly different with respect to the values for other injected agents at the indicated significance level. Brackets with asterisks above them indicate statistical significance between the shown pairs.

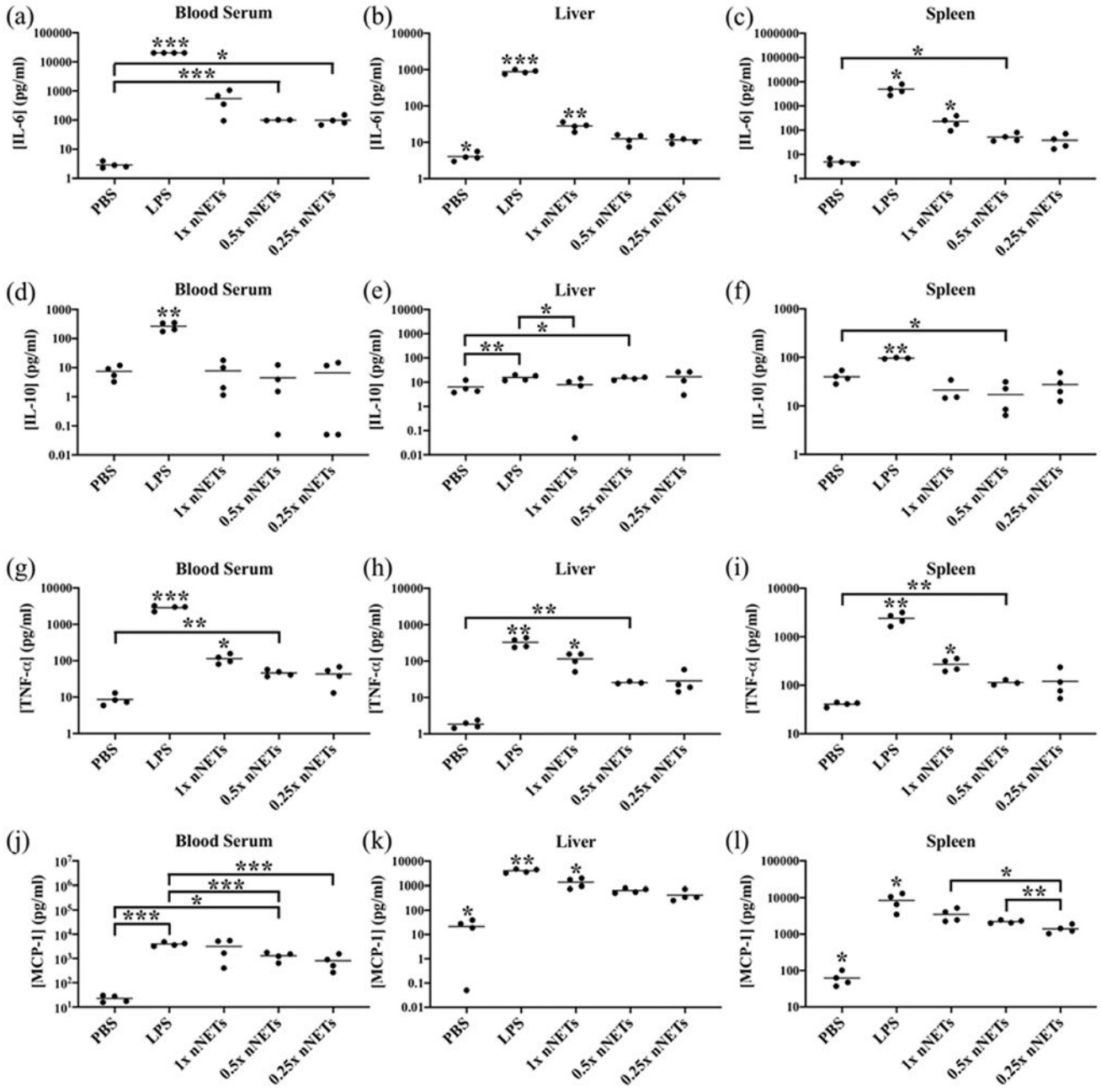

Figure 2.

Effects of nNET dose on cytokine production at 2 h post-tail vein injection. Cytokine concentration measurements (as represented by dots) for (a–c) IL-6, (d–f) IL-10, (g–i) TNF-α, and (j–l) MCP-1 in the blood serum, liver, and spleen, respectively, are shown with the population mean (horizontal bars). PBS and LPS correspond to negative and positive controls, respectively. Statistical significance of * ($p < 0.05$), ** ($p < 0.01$), and ***($p < 0.001$) are indicated. Significance markings directly above a given agent indicate that the mean value for that agent is significantly different from all other agents

at the indicated significance level. Brackets with asterisks above them indicate statistical significance between the shown pairs.

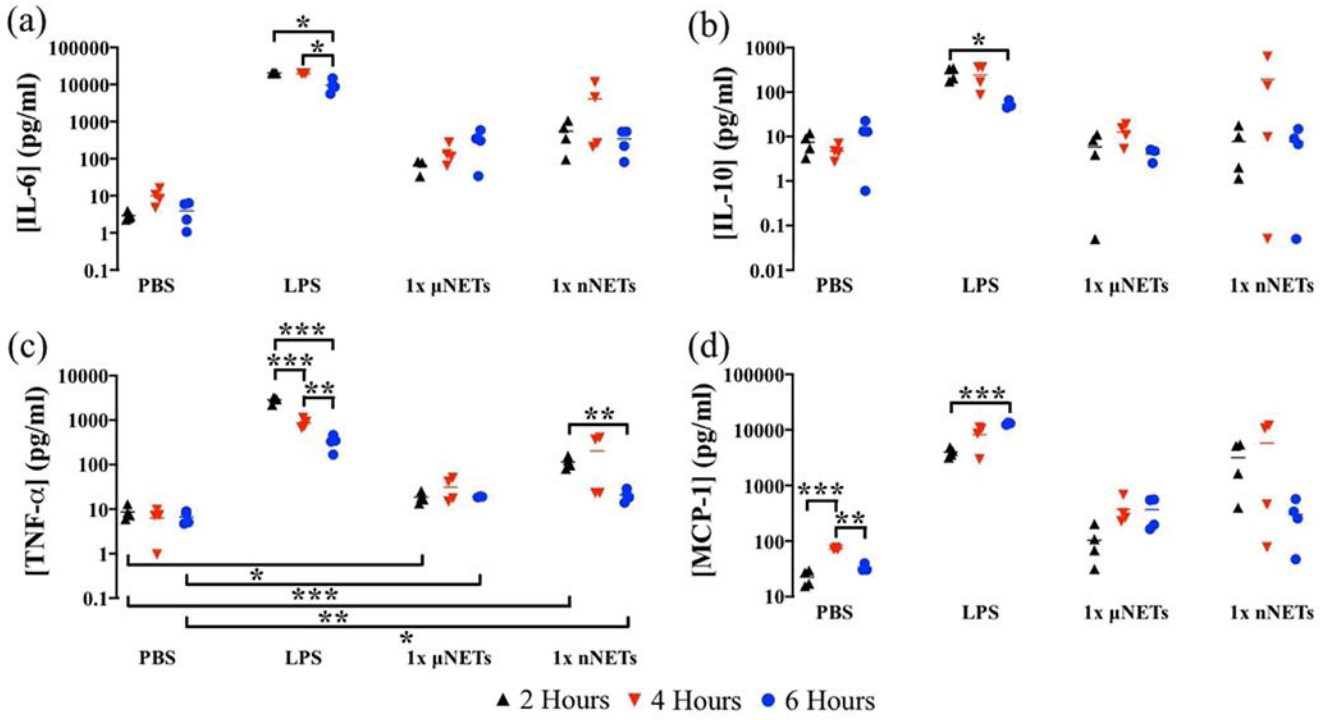

Figure 3.

Concentration of cytokines in blood serum at 2, 4, and 6 h postinjection of PBS, LPS, 1× μNETs, and 1× nNETs. Concentration measurements (as represented by symbols) for (a) IL-6, (b) IL-10, (c) TNF-α, and (d) MCP-1 are shown with the population mean (horizontal bars). Statistical significance of * ($p < 0.05$), ** ($p < 0.01$), and ***($p < 0.001$) are indicated. Brackets with asterisks above them indicate statistically significant differences between the shown pairs.

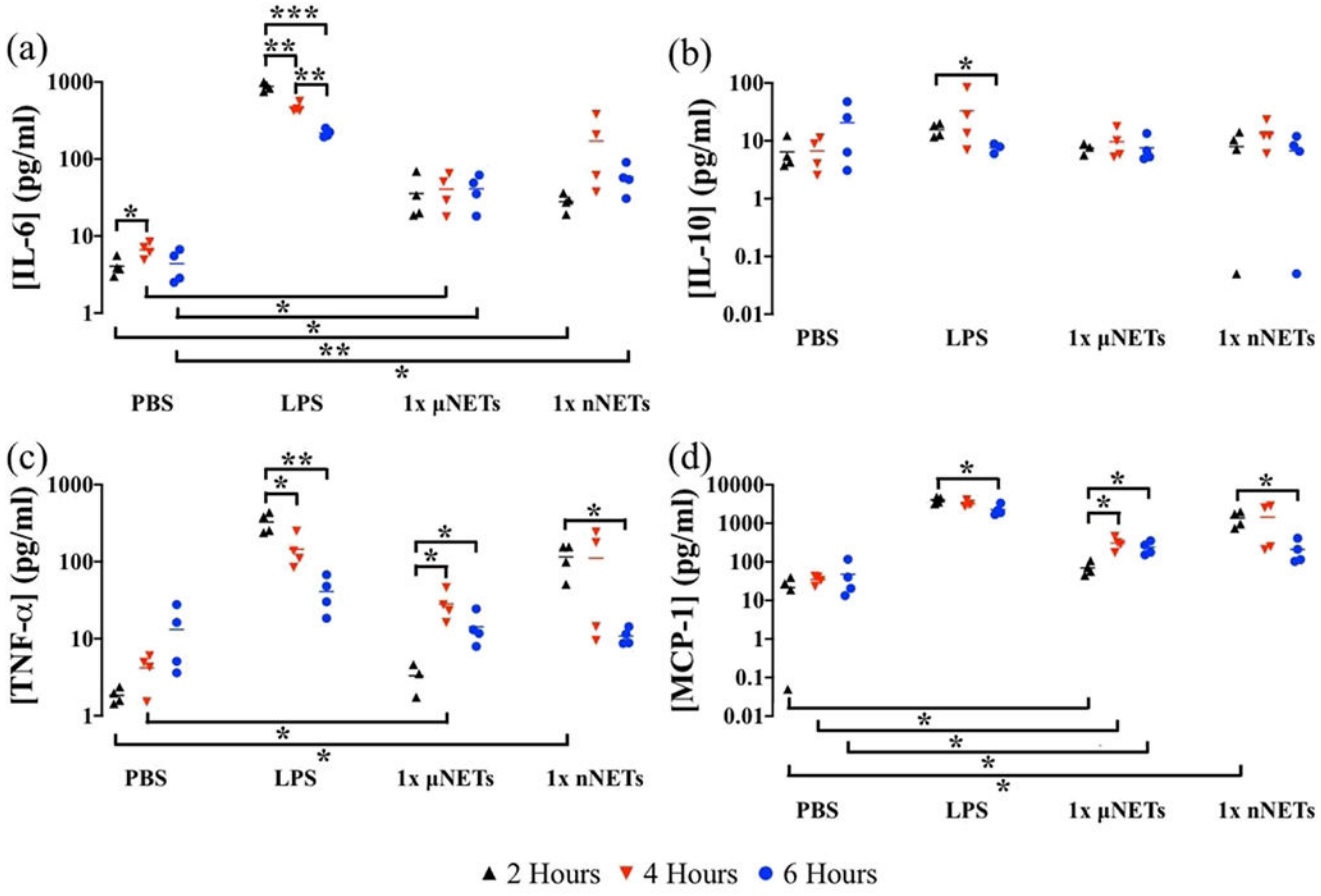

Figure 4.

Concentration of cytokines in the liver at 2, 4, and 6 h postinjection of PBS, LPS, 1× μNETs, and 1× nNETs. Concentration measurements (as represented by symbols) for (a) IL-6, (b) IL-10, (c) TNF-α, and (d) MCP-1 are shown with the population mean (horizontal bars). Statistical significance of * ($p < 0.05$), ** ($p < 0.01$), and ***($p < 0.001$) are indicated. Brackets with asterisks above them indicate statistically significant differences between the shown pairs.

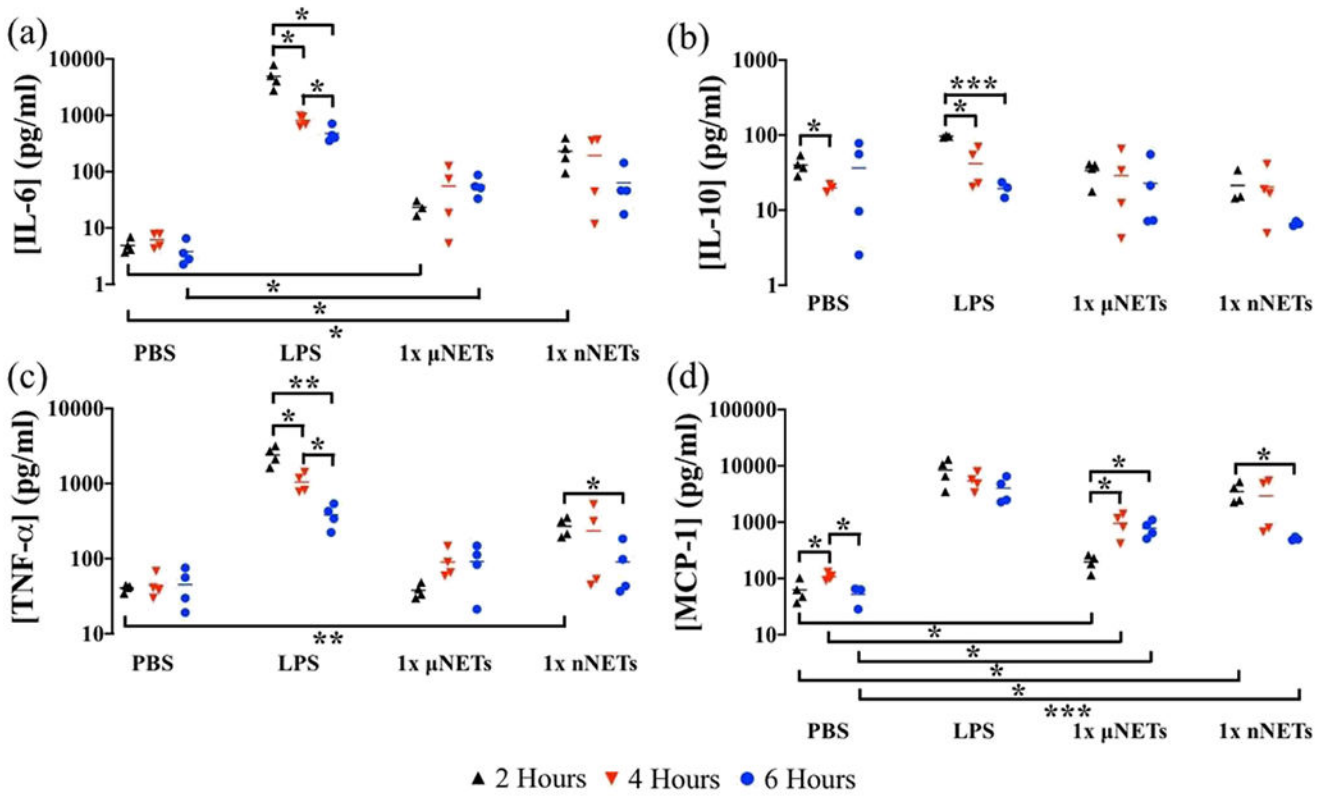

Figure 5.

Concentration of cytokines in the spleen at 2, 4, and 6 h postinjection of PBS, LPS, 1× μNETs, and 1× nNETs. Concentration measurements (as represented by symbols) of (a) IL-6, (b) IL-10, (c) TNF-α, and (d) MCP-1 are shown with the population mean (horizontal bars). Statistical significance of * ($p < 0.05$), ** ($p < 0.01$), and ***($p < 0.001$) are indicated. Brackets with asterisks above them indicate statistically significant differences between the shown pairs.

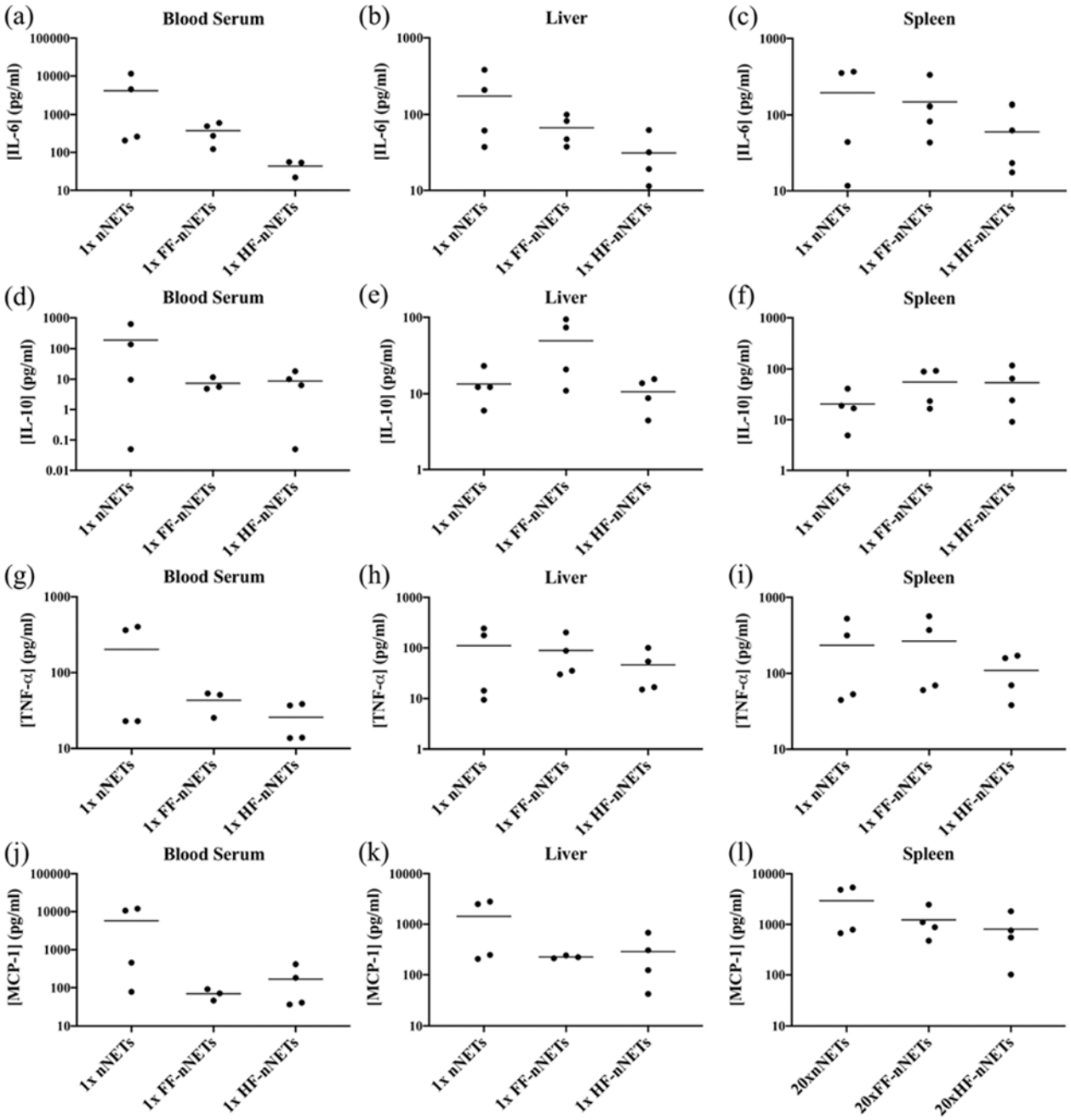

Figure 6.

Concentration of cytokines at 4 h postinjection of 1× nNETs, 1× FF-nNETs, and 1× HF-nNETs. Concentration measurements (represented as dots) for (a–c) IL-6, (d–f) IL-10, (g–i) TNF-α, and (j–l) MCP-1 in the blood serum, liver, and spleen, respectively, are presented. Horizontal bars represent the mean values associated with a given cytokine concentration.

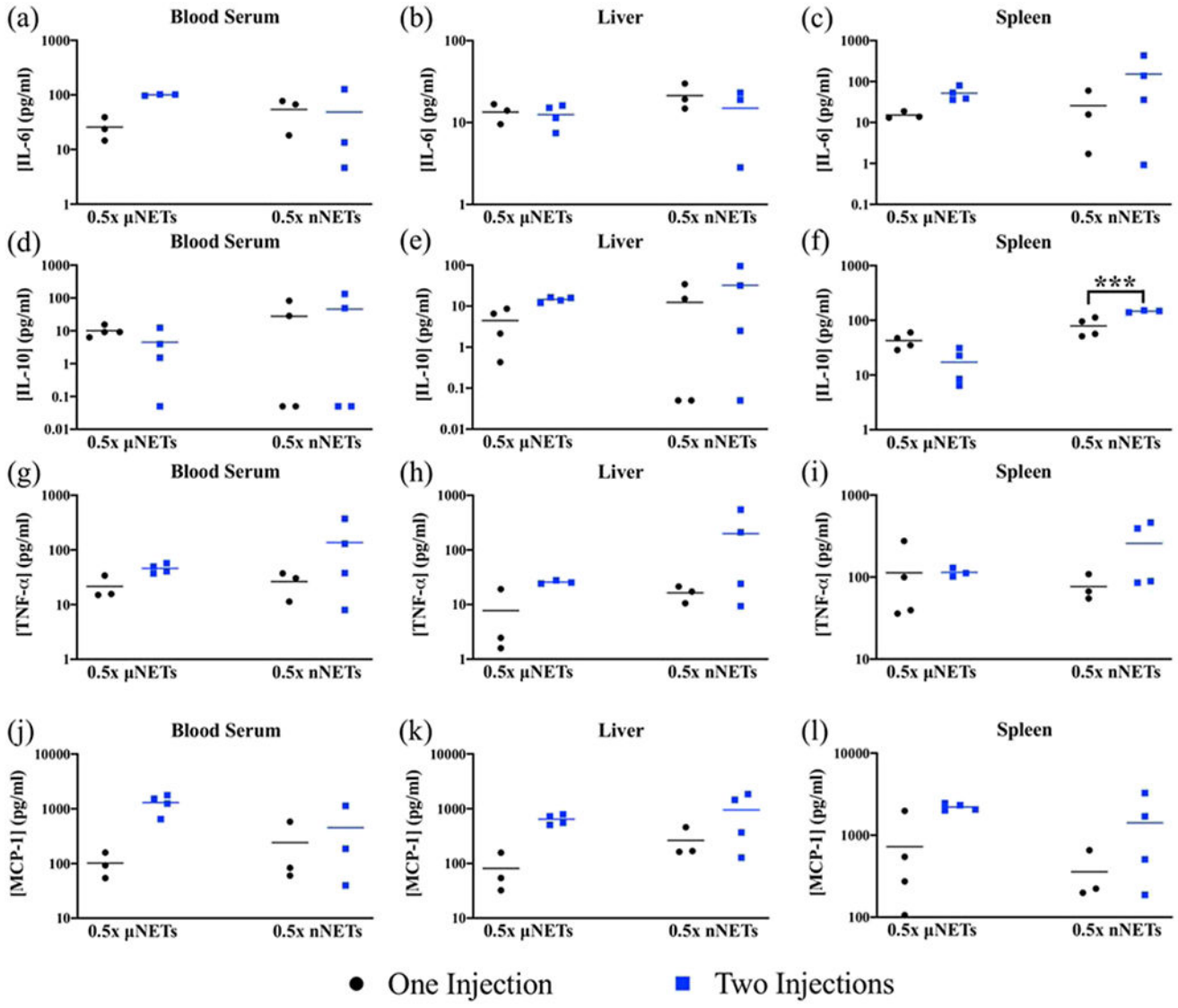

Figure 7.

Effect of dual injections of 0.5× μNETs and 0.5× nNETs one week apart. Cytokine measurements were made using samples collected 2 h after the second injection. Concentration measurements (represented as symbols) for (a–c) IL-6, (d–f) IL-10, (g–i) TNF-α, and (j–l) MCP-1 in the blood serum, liver, and spleen, respectively, are presented. Horizontal bars represent the mean values associated with a given cytokine concentration. Bracket with *** asterisks above it indicates statistically significant differences between the shown pairs ($p < 0.001$). None of the other t-tests resulted in statistically significant p-values. Therefore, statistical significances of $p < 0.05$ and $p < 0.01$ are not indicated.

Table 1.

Description of the Acute Immunogenicity Studies

immunogenicity study	administered particle	particle relative dose (relative number concentration)	euthanasia time point after particle injection	statistics
effect of particle size and dose	μNETs, nNETs	1×, 0.5×, 0.25×	2 h	•Brown–Forsythe one-way ANOVA, and Welch one-way ANOVA followed by unpaired Welch's *t*-tests (two-tailed unless otherwise noted) •one-tailed unpaired Welch's *t*-test for comparisons to LPS, and comparisons between doses of the same construct
time-dependent cytokine response	μNETs, nNETs	1×	2, 4, 6 h	•Brown–Forsythe one-way ANOVA, and Welch one-way ANOVA followed by unpaired Welch's *t*-tests (two-tailed unless otherwise noted) •one-tailed unpaired Welch's *t*-test for comparisons to LPS (except comparisons between LPS at different time points)
effects of nNET functionalization with folate or Herceptin	FF-nNETs, HF-nNETs	1×	4 h	•Brown–Forsythe one-way ANOVA and Welch one-way ANOVA followed by unpaired two-tailed Welch's *t*-tests
effects of dual injections of NETs one week apart	μNETs, nNETs	0.5×	2 h after second injection	•unpaired two-tailed Welch's *t*-tests

Table 2.

Key Findings Associated with the Acute Immunogenicity Studies

immunogenicity study	key findings
effect of particle size and dose	•mean concentrations of IL-6, IL-10, TNF-α, and MCP-1 in blood serum, the liver, and the spleen were significantly lower than the corresponding LPS-induced concentrations at all investigated μNET relative doses •although there were some increases in the mean concentrations of IL-6, IL-10, TNF-α, and MCP-1 relative to those induced by PBS, in general, they did not appear to correlate with the investigated μNET doses, possibly because of the variabilities in response among animals •mean concentrations of IL-6 in blood serum, the liver, and the spleen in response to the investigated nNET doses were significantly belowLPS-induced concentrations • 1× nNETs induced significantly higher concentrations of TNF-α as compared to 0.5× nNETs and 0.25× nNETs in blood serum, the liver, and the spleen •all investigated nNET doses induced significantly higher concentrations of MCP-1 in the liver and spleen as compared to PBS •mean concentrations of IL-6 and IL-10 in blood serum, the liver, and the spleen did not significantly change at 2, 4, and 6 h postinjection of either 1× μNETs or 1× nNETs •mean concentrations of TNF-α and MCP-1 in blood serum did not significantly change at 2, 4, and 6 h postinjection of 1× μNETs •mean concentrations of TNF-α and MCP-1 in the liver were significantly higher at 4 and 6 h postinjection of 1× μNETs as compared to their corresponding values at 2 h
time-dependent cytokine response	•mean concentration of MCP-1 in the spleen at 4 and 6 h postinjection of 1× μNETs was significantly higher than its respective concentration at 2 h, and at all three time points, the 1× μNETs induced significantly higher levels of McP-1 as compared to PBS •mean concentrations of TNF-α in blood serum, the liver, and the spleen at 6 h postinjection of 1× nNETs were significantly lower than their respective concentrations at 2 h •mean concentrations of MCP-1 in the liver and spleen at 6 h postinjection of 1× nNETs were significantly lower than their respective concentrations at 2 h, but not significantly different from PBS-induced MCP-1 concentration in the liver at 6 h
effects of nNET functionalization with folate or Herceptin	•functionalization of nNETs was associated with a general trend in reduction of IL-6 and MCP-1 concentrations in blood serum, the liver, and the spleen, and TNF-α and IL-10 concentration reduction in blood serum
effects of dual injections one week apart	•with the exception of IL-10 in the spleen in response to nNETs, the second injection of 0.5× μNETs or 0.5× nNETs did not result in statistically significant changes in concentrations of other cytokines as compared to a single injection